POLITECNICO DI TORINO
Repository ISTITUZIONALE

Analysis of the optical gain characteristics of semiconductor quantum dash materials including the band structure modifications due to the wetting layer

(Article begins on next page)

25 April 2024

Analysis of the Optical Gain Characteristics of Semiconductor Quantum-Dash Materials Including the Band Structure Modifications Due to the Wetting Layer

Mariangela Gioannini

Abstract—**We present a numerical model for the calculation of the opto-electronic properties of a semiconductor InAs–InAlGaAs quantum dash active material including the presence of the wetting layer (WL), formed at the bottom of the dashes, and the quantum mechanical coupling among dashes caused by the high density of the InAs islands. The model calculates self-consistently the conduction and valence band energy diagram of the confined and unconfined states, the corresponding density of states, the electron and hole wavefunctions and the gain spectra. The results obtained are also compared with a more simple model that consider dashes as isolated and without the WL. The comparison evidences the role of the WL in limiting the gain performance such as the maximum gain, the differential gain and the optical gain bandwidth. The numerical tool is then used to design an improved quantum dash material, which allows to overcome these gain limitations even in presence of the WL and the high dash density.**

Index Terms—**Modeling, optical gain, quantum-dash laser and optical amplifiers, self-assembled quantum dash.**

I. INTRODUCTION

NANOSTRUCTURE semiconductor materials, quantum dots (QD), [1], quantum dash (QDash) [2], and quantum wire (QWR) have been the focus of many experimental and theoretical works in the recent years and in particular QD and QDash material have shown very promising application in semiconductor laser and optical amplifiers [3]. The advantage of the nanostructure active region consists indeed in the possibility of tailoring the gain properties by engineering the growth process. For example several experiments have shown that a properly designed QD or QDash material can give wide emission spectra and can be successfully used in broad-band superluminescent diodes [4] or as active waveguide for external cavity tunable lasers [5] and broad-band optical amplifiers [6], [7]. For these applications, requiring large optical bandwidth, it is necessary to grow nanostructures that allow the presence of at least one excited state confined in the QDs [8], because the δ-like density of states allows to invert the ground state and populate the excited states at fairly low current densities

[9] compared with the multiquantum-well design [10]. Furthermore, the fabrication procedure, based on a self-assembled process, gives an inhomogeneous gain broadening due to size fluctuations, that permits the continuous coverage of the whole gain bandwidth. However, in the self-assembled process a thin wetting layer always exists as a uniform film at the bottom of the assembled quantum islands [11]. The presence of the WL influences significantly the confinement of the carriers in the excited states and can reduce the emission performance. It was shown that it limits the maximum achievable gain at room temperature [12], significantly influences the dynamic performance of the lasers [13] and modifies the carrier confinement in the dots [14]. Despite the importance of the WL, the various models presented in the literature to investigate the electrical and optical properties of the nanostructure materials do not evaluate self-consistently the energy band diagram of the dot, wetting layer and barrier system. In many cases the nanostructures are also considered as isolated (one single dot or dash surrounded by the barrier material); but when their density is rather high (e.g., high filling factor to get enough modal gain) the quantum mechanical coupling among the nanostructures can not be neglected. Such coupling is further enhanced by the presence of the WL.

A second aspect frequently neglected in QD laser modeling is the presence of the barrier state due to the spacer that separates the various QD layers. At the high pumping rate, necessary to invert the excited states, the barrier can trap the carriers and reduce the injection efficiency of electrons and holes in the zero-dimensional confined states; the carrier density present in the barrier can also give additional loss due to free-carrier and intervalence band absorption [15].

The aim of this work is to present a detailed numerical model for the calculation of the optoelectronic properties and emission characteristics of the recently realized InAs–InAlGaAs QDash material [7] including properly the presence of the WL and the barrier, by computing the energy band diagram of the whole structure. This approach will then be used to design a new QDash material structure with improved optical bandwidth. We first quantitatively compare two QDash models: the single-isolated dash model (i.e., just one QDash surrounded by the InAlGaAs barrier) and the more realistic model that includes the presence of the WL and the quantum mechanical coupling among adjacent dashes, caused by the high density of dashes [2]. Through our calculations we highlight how the WL
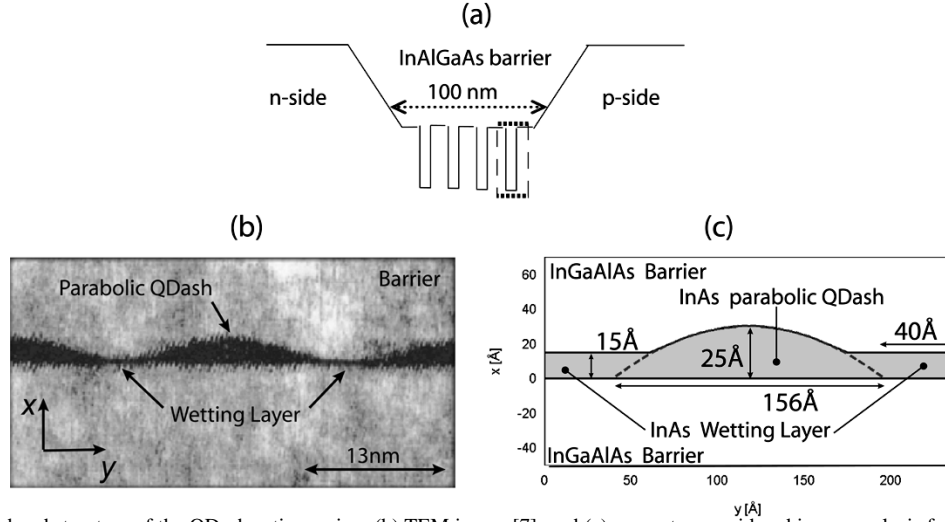
Fig. 1.   (a) Conduction band structure of the QDash active region, (b) TEM image [7], and (c) geometry considered in our analysis for the dash with WL model (solid line) and the single isolated dash model (dashed line).

changes the conduction and valence bands energy diagrams, the electron confinement in the dashes and the density of states in conduction band (CB) and valence band (VB) with respect to the isolated dash case. We then evaluate the gain spectra and show that some important gain properties such as the optical gain bandwidth, the maximum gain and the differential gain are negatively influenced by the WL. Since it is not possible to eliminate the WL, we will then show the results for an improved QDash structure that overcomes these limitations. The paper is organized as follows. in Section II, we present our numerical model. In Section III, we discuss some numerical results and propose a new design of the dash material. Finally, in Section IV, we draw the conclusions.

II. NUMERICAL MODEL

In this section, we present in detail the numerical model for the self-consistent calculation of the QDash material confined and unconfined states, of the density of states and of the gain spectra including the WL. The model, starting from the knowledge of the composition and dash geometry obtained from SEM and TEM images [7], calculates the CB and VB energy diagram solving the Schrödinger equation using the single particle effective mass approximation. Such calculation allows also to obtain numerically the equivalent parameters necessary to model correctly the WL state.

To keep our model as simple as possible and focus exclusively on the effect of the WL, we have neglected the coupling between the bands and we have used a single band Schrödinger equation to calculate the electron and heavy hole states in CB and VB. The deformation potential induced by the strain was included only empirically by modifying, respect to the bulk case, the InAs CB and VB band-edges and the energy gap and by introducing two different hole effective masses: one in the growth plane (parallel direction) and another one in the direction perpendicular to it. The parameters used for these very approximate assumptions where obtained in [16] through the fitting of the calculated amplified spontaneous emission and gain spectra with the experimental data. The results obtained are, therefore, strongly dependent on these severe assumptions and on the choice of the pa-

rameters used in the single particle model. Although a rigorous strain calculation and an $8 \times 8 \, \mathbf{k} \cdot \mathbf{p}$ solution of the Hamiltonian equation [17] allows to obtain a more quantitative accurate reference solution, we believe it should not change, for this particular structure, the general qualitative conclusions obtained applying the single particle effective mass model. Using the device simulator "next $\mathbf{nano}^3$" [18], we have, for example, verified tha for the particular InAs–InAlGaAs QDash material considered here, the hydrostatic strain is almost constant, concentrated in the InAs dash cross section and it causes a variation of the CB and VB edges of nearly the same entity as the one set empirically.

A. QDash Waveguide Structure

The QDash material we consider first is the same presented in [2]; the conduction band diagram of the active region is schematized in Fig. 1(a). The optical waveguide consists of an InAlGaAs graded index separate confinement heterostructure and the active region is formed by InAs QDash layers [one layer in the dotted area of Fig. 1(a)] separated by a 25-nm $In_{0.528}Al_{0.238}Ga_{0.234}As$ barrier; the total barrier thickness is about 100 nm. In [19], it was demonstrated that since dashes are elongated (100–200 nm) InAs islands, the QDash material has almost a quantum-wire nature and the confinement in the longitudinal direction can be neglected. Therefore, in our model we approximate the dashes with wires and we concentrate only on the carrier confinement in the transversal direction.

In Fig. 1(b), we show a TEM cross section of one self-assembled QDash layer [7] and in Fig. 1(a), we plot in solid line the corresponding transversal dash geometry considered for our calculation. We have included the WL, clearly visible in the TEM image, as a thin InAs film at the bottom of the dashes. The TEM image in Fig. 1(b) also shows that the separation between adjacent dashes in the y direction is much smaller than the dash width and, therefore, the quantum mechanical coupling among the adjacent dashes is not negligible. In Fig. 1(c), we also report in dashed line the geometry representing a single isolated dash without WL. In [16], we have shown that the length and width fluctuations of the dash size do not affect significantly the

emission characteristics, whereas the dash height variation is the most important parameter to guarantee enough inhomogeneous broadening for a continuous coverage of the gain bandwidth. In our calculation we will, therefore, consider only the fluctuations of the dash height whereas the dash width is fixed to 15.6 nm.

B. Modeling of the WL and Dash Coupling

In the literature to calculate the carrier filling of the confined states and the consequent gain spectrum, the presence of the WL is usually included as a generic state with a proper effective degeneracy, estimated from the two dimensional density of states [20]. The WL state energy is typically set equal to the energy of the CB and VB band edge (barrier energy) or empirically just below it. Since most of these models consider only the ground state, they neglect the effects introduced by the WL and by the high dash density on the other higher energy states. With this approximation it is assumed that each nanostructure behaves independently on the ensemble in which it is grown. On the contrary we have found that in a realistic QDash material the high dash density (more than 50%) and the presence of the WL significantly alter the electronic properties. In particular the electron excited states with energy well below the InAlGaAs barrier band edge start being unbounded. This facilitates the quantum mechanical coupling among close adjacent dashes and causes the electron wavefuctions to be no longer localized in a single dash. On the other hand the corresponding hole excited state still remains well confined in the dash, thanks to the higher hole effective mass. A self-consistent modeling of the whole dash ensemble is thus necessary to calculate the gain spectra in these more realistic conditions. At this purpose, we need the correct energy position of the confined and unconfined states and the corresponding density of states to determine the carrier distribution among the states at room temperature.

To calculate the energy band structure of the ensemble including the WL and the dash quantum mechanical coupling, we neglect the dash stochastic distribution assuming that the dashes, all of same size, are displaced in a periodic array.

The energy of the states confined in the dashes or in the WL and their corresponding wavefunctions have been obtained solving the single particle Schrödinger equation in the effective mass approximation in a two dimensional potential periodic in y [see Fig. 1(b)]. The structure shown in Fig. 1(c) is thus the elementary cell of the periodic array. The particle wavefunction $\psi_{n,k_y}(x,y)$ of the nth band in a two-dimensional (2-D) potential, periodic in y with period L, can be written as $\psi_{n,k_y}(x,y) = (1/L)u_{n,k_y}(x,y)e^{-jk_y y}$, where $u_{n,k_y}(x,y)$ is a periodic function that satisfies the Bloch theorem $u_{n,k_y}(x,y+L) = u_{n,k_y}(x,y)$. Substituting $\psi_{n,k_y}(x,y)$ in the single particle Schrödinger equation we obtain a partial differential equation for $u_{n,k_y}(x,y)$

$$-\frac{\hbar^2}{2m_x}\frac{\partial^2 u_{n,k_y}(x,y)}{\partial x^2} - \frac{\hbar^2}{2m_y}\frac{\partial^2 u_{n,k_y}(x,y)}{\partial y^2}$$
$$-2jk_y\frac{\hbar^2}{2m_y}\frac{\partial u_{n,k_y}(x,y)}{\partial y}$$
$$+\left(k_y^2\frac{\hbar^2}{2m_y}+V(x,y)\right)u_{n,k_y}(x,y) = W_{n,k_y}u_{n,k_y}(x,y)$$

(1)

where $m_{x,y}$ are the particle effective mass in the x and y directions to account for the modification induced by the strain; $V(x,y)$ is the 2-D potential, and W_{n,k_y} is the corresponding energy eigenvalue for the state with wavevector k_y in the nth band. In this model, we apply this equation to both electrons and heavy holes, neglecting the coupling with the light holes and split-off bands. In presence of compressive strain—as for the material system we consider—these two bands are indeed split far away from the VB band edge and play, therefore, a less significant role. Performing a rigorous strain calculation [18] we have indeed verified that the light hole and split-off bands in the InAs material are, respectively, 150 and 500 meV apart from the top of the heavy hole energy.

To include the effect of the dash coupling in the calculation of the CB and VB energy diagram, (1) has been solved for each value of the momentum k_y using a finite element method and setting periodic boundary condition at the left and right hand border of the cell in Fig. 1(c). In the case of the single isolated dash without WL [dashed shape in Fig. 1(c)] the equation was solved only for $k_y = 0$ and the left and right borders were pushed further away imposing Dirichelet boundary conditions (wavefunctions null at the borders).

C. Calculation of the Gain Spectra

The solution of (1) in presence of the WL and dash coupling shows (see Section III-A) that the QDash material under investigation [2] has one state well confined in the dashes [the ground state (GS)], one excited state (ES) strongly confined for the holes but significantly coupled with the adjacent dashes for the electrons, a WL, and a barrier state. To calculate the gain spectra we have then to account for the recombination in the GS, ES, and WL. The net modal gain is, therefore, given by

$$g_{net}(\lambda) = \Gamma_{wire}[g_{GS_{conf,conf}}(\lambda) + g_{ES_{unconf,conf}}(\lambda)]$$
$$+ \Gamma_{WL}g_{WL}(\lambda) - \alpha_i - \Gamma_{barrier}\alpha_{barrier} \quad (2)$$

where $g_{GS,ES}$ represents the GS and ES recombination and the subscript conf or unconf are used to stress the fact that the recombination may occur between electron and hole states that are both well confined in the dashes (conf, conf) or unconfined in CB and confined in VB (unconf, conf). In the case of the single isolated dash without WL, both GS and ES electrons are well localized in the dashes and the ES contribution to the gain is $g_{ES_{conf,conf}}$. The contribution due to the WL is g_{WL}; α_i is the internal modal loss.

As reported in [21], the net modal gain of the reduced dimensionality active regions (wire and WL) has been calculated simply by multiplying the material gain ($g_{GS,ES}$ and g_{WL}) with the optical confinement factors Γ_{wire} and Γ_{WL} resulting by the overlap integral of the electric field with the wire and WL cross sections, respectively. For the calculation of Γ_{wire} and Γ_{WL} we have, respectively, used an average wire cross section $\overline{A}$ and a WL thickness of d_{WL}.

The carrier density accumulated in the InAlGaAs barrier can also give an additional contribution to the loss ($\alpha_{barrier}$), due to free-carrier and intervalence band absorption written as: $\alpha_{barrier} = k_n n_{barrier} + k_p p_{barrier}$ [22], where $n, p_{barrier}$ are the electron and hole density per unit volume in the barrier. Since the confinement factor of the optical field in the barrier region,

TABLE I
QDASH MATERIAL PARAMETERS

In$_{0.528}$Al$_{0.238}$Ga$_{0.234}$As barrier	
m_e^*	$0.059m_0$
m_h^*	$0.43m_0$
InAs QDash and WL	
m_e^*	$0.04m_0$
$m_{hh,\parallel}^*$	$0.32m_0$
$m_{hh,\perp}^*$	$0.538m_0$
Conduction band edge, ΔE_{CB}, respect to the bottom of the InAs CB energy	391 meV
Valence band edge, ΔE_{VB}, respect to the top of the InAs VB energy	210 meV

Γ_{barrier}, is much higher than the confinement factor in the dashes (about ten times in the QDash waveguide we consider), the influence of this additional loss is stronger than in quantum well or bulk materials [15] and can not be neglected.

The material gain from each type of recombination in (2) is calculated according to the density matrix theory [23]. In this analysis, we calculate only the TE gain because the dashes are oriented parallel to the TE optical field and the TM contribution is negligible being the dash width much larger than the dash height [23].

For GS and ES recombination of type conf, conf the gain is calculated assuming a quantum wire assembly with inhomogeneous wire distribution; therefore, the wire populations is divided in N_{wire} groups, each with an existence probability $P_{\text{wire},j}$, with j indicating the jth group. $P_{\text{wire},j}$ is calculated assuming a Gaussian distribution of the dash height. The material gain is then given by the sum of the contribution of each group

$$g_{\text{GS,ES}_{\text{conf,conf}}} = \frac{C_g}{\hbar\omega} \cdot \sum_{j=1}^{N_{\text{wire}}} P_{\text{wire},j} \int M_b^2 I_{j_{\text{conf,conf}}}^2 \rho_{\text{wire},j}(\varepsilon)$$
$$\times [f_e(\varepsilon_e) + f_h(\varepsilon_h) - 1] L(\hbar\omega - \varepsilon) d\varepsilon \quad (3)$$

where C_g is a constant [16], M_b^2 is the transition matrix element given by the interband matrix element [24], and $I_{j_{\text{conf,conf}}}^2$ is the overlap integral of the envelope functions $\psi_{e,h}(x,y)$ of the electron and hole of the jth wire involved in the transition. $L(\hbar\omega - \varepsilon)$ is the homogenous broadening function [23], $f_{e,h}$ are the electron and hole occupation probability. In (3), ε is the energy of the recombination between an electron with energy ε_e and a hole with energy ε_h: $\varepsilon = \varepsilon_h + \varepsilon_e + E_g$. These energies are given by:

$$\varepsilon_{e,h} = \varepsilon_{\text{GS,ES}_{j_{e,h}}} + \frac{\hbar^2}{2m_{e,h}} k_z^2 \quad (4)$$

with $\varepsilon_{\text{GS,ES}_{j_{e,h}}}$ the energy of the GS or ES confined in CB or VB in the jth wire group obtained by the solution of (1) and k_z the momentum along the wire direction z. Finally, $\rho_{\text{wire},j}$ is the reduced density of states for the jth wire

$$\rho_{\text{wire},j} = \frac{1}{\pi \bar{A}} \left(\frac{2m_r}{\hbar^2}\right)^{1/2} \frac{1}{\sqrt{\varepsilon - \varepsilon_{\text{GS,ES}_j}}} \quad (5)$$

with $\varepsilon_{\text{GS,ES}_j} = \varepsilon_{\text{GS,ES}_{j_e}} + \varepsilon_{\text{GS,ES}_{j_h}} + E_g$.

We have seen that in the case of recombination from the ES of type unconf, conf caused by the presence of the WL and the

dash coupling, the inhomogeneous linewidth due to size fluctuations is comparable with the homogeneous broadening, therefore, for this recombination, we can neglect the stochastic size distribution in the gain calculation. Since in this case the electrons of the ES in CB are strongly coupled with the adjacent dashes, the ES degenerates in a mini-band (see Section III-A) whose energy and wavefunction depend on k_y: $\varepsilon_{\text{ES},e}(k_y)$ and $\psi_{\text{ES},e}(x,y,k_y)$. Therefore, the gain has to be calculated numerically starting from the knowledge of these relations, obtained by the solution of (1). Assuming the $\mathbf{k}$ selection rule valid, the material gain at the recombination energy ε is given by the sum of all the recombination between the electron state in CB with energy

$$\varepsilon_e(k_y, k_z) = \varepsilon_{\text{ES},e}(k_y) + \frac{\hbar^2}{2m_e} k_z^2 \quad (6)$$

and the hole state VB with energy

$$\varepsilon_h(k_y, k_z) = \varepsilon_{\text{ES},h} + \frac{\hbar^2}{2m_h} k_z^2 \quad (7)$$

such that $\varepsilon = \varepsilon_e(k_y, k_z) + \varepsilon_h(k_y, k_z) + E_g$. In (7), we have omitted the dependence of $\varepsilon_{\text{ES},h}$ on k_y because the ES holes are well localized in the dash.

Including the homogeneous broadening the gain is given by

$$g_{\text{unconf,conf}}(\hbar\omega) = \frac{C_g}{\hbar\omega} \int\int_{k_y,k_z} \frac{L}{2\pi^2 \bar{A}} M_b^2 I_{\text{unconf,conf}}^2(k_y)$$
$$\cdot [f_e(\varepsilon_e) + f_h(\varepsilon_h) - 1] L(\hbar\omega - \varepsilon) dk_y dk_z \quad (8)$$

where $I_{\text{unconf,conf}}^2$ is the overlap integral between the electron and hole wavefunction involved in the transition and it depends on k_y due to the dependence on k_y of the electron wavefunction.

Finally the contribution of the WL is calculated assuming that the WL state has a 2-D dimensionality

$$g_{\text{WL}} = \frac{C_g}{\hbar\omega} \cdot \int M_b^2 I_{\text{WL}}^2 \rho_{\text{WL}}(\varepsilon) [f_e(\varepsilon_e) + f_h(\varepsilon_h) - 1] L(\hbar\omega - \varepsilon) d\varepsilon \quad (9)$$

where $\rho_{\text{WL}}(\varepsilon)$ is the 2-D reduced density of states given by

$$\rho_{\text{WL}}(\varepsilon) = \frac{m_{2D_r}}{\pi\hbar^2 d_{\text{WL}}} u(\varepsilon - \varepsilon_{\text{WL}}) \quad (10)$$

where $u(\varepsilon)$ is the step function, ε_{WL} is the recombination energy from the WL and m_{2D_r} is WL reduced effective mass
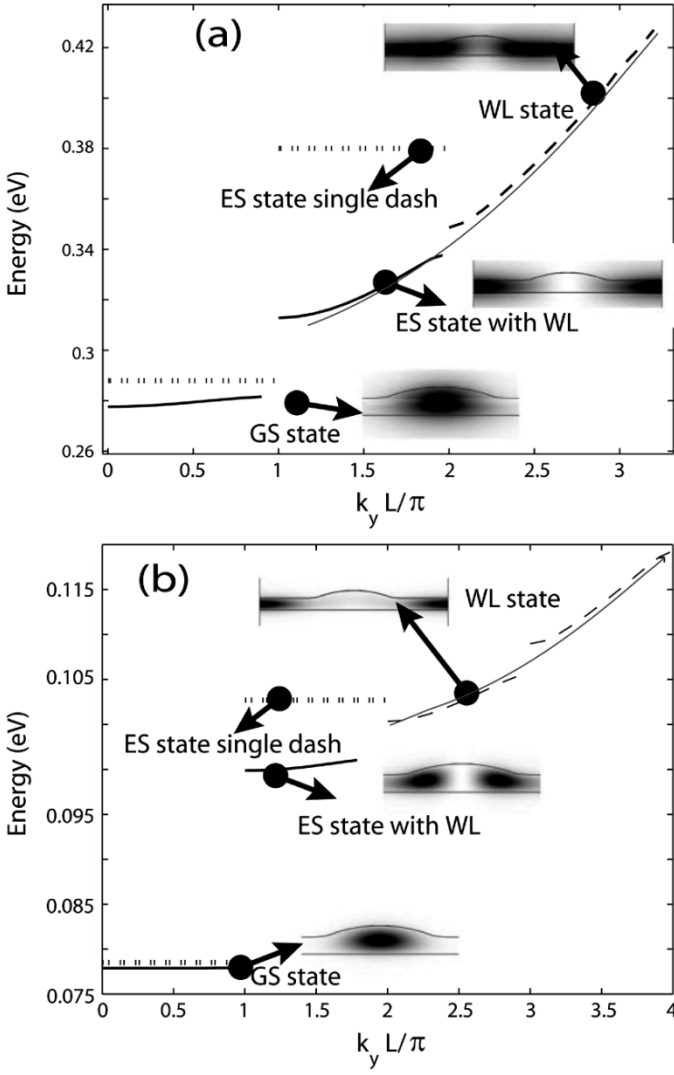
Fig. 2. (a) CB and (b) VB energy diagram of the structure shown in Fig. 1(c), obtained with the single isolated dash model (thick dotted line) and the dash coupling with WL model (solid line and dashed line for WL states). The figures in the insets show for each mini-band the corresponding wavefunctions. The thin solid line is the fitting of the unconfined states relation dispersion with a parabolic function.

obtained from the WL electron and hole equivalent effective masses m_{2D_e} and m_{2D_h}. The parameters characterizing the WL are, therefore, ε_{WL}, m_{2D_e} and m_{2D_h}, which are obtained from the fitting of the computed CB and VB energy diagrams as shown later in Section III-A.

D. Calculation of the Occupation Probability f_e and f_h

The presence of the WL and barrier states also affects the dash filling when the carrier injection is increased. In our model this is taken into account through the occupation probabilities f_e and f_h. They are calculated assuming that at room temperature and in absence of stimulated emission the electron and hole population equilibrate in each QDash layer, with the WL and the barrier states [20]. The occupation are thus defined through the Fermi distributions determined by the electron and hole quasi-Fermi
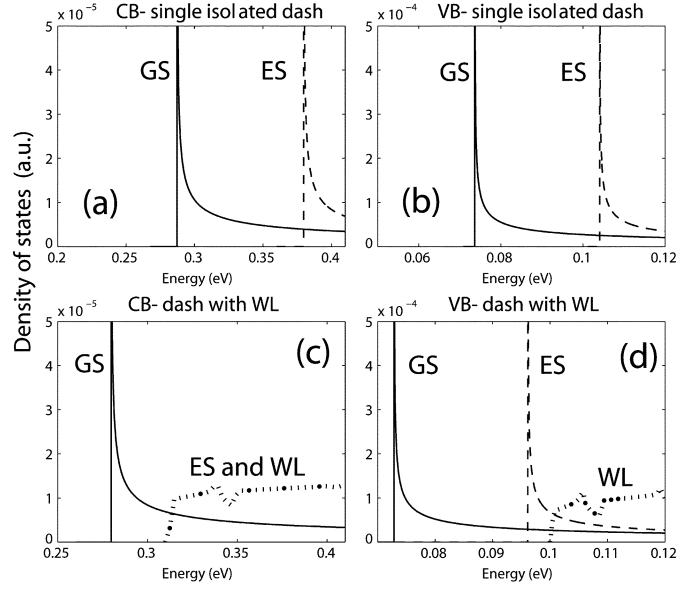

Fig. 3. (a) Density of states in CB and (b) in VB calculated with the single isolated dash model: solid line GS contribution; dashed line ES contribution. DOS with WL and dash coupling in (c) CB and (d) in VB; the dashed line in (c) is the sum of the unconfined ES and WL contribution; the dotted line in (d) is only the WL contribution.

levels E_{Fe} and E_{Fh}, calculated setting the neutrality condition to a unit area of the waveguide [25]

$$N_L N_s n_{Qdash} + N_L n_{unconf} + n_{barrier}$$
$$= N_L N_s p_{Qdash} + N_L p_{unconf} + p_{barrier} \quad (11)$$

where N_L is the number of wire layers and N_s is the wire density per layer. In (11), n_{Qdash} is the density of electrons per unit length in the states confined in the wires (i.e., GS and ES in the case of the single isolated dash, GS only when the presence of the WL and dash coupling is considered) and p_{Qdash} is the density of hole confined in the dashes (i.e., GS and ES in both models). These carrier density are calculated referring to the dash of average size

$$n, p_{QDash} = \sum_{GS,ES} \int_{\bar{\varepsilon}_{GS,ES_{e,h}}}^{\infty} \frac{1}{\pi} \left(\frac{2m_{e,h}}{\hbar^2} \right)^{1/2}$$
$$\times \frac{1}{\sqrt{\varepsilon - \bar{\varepsilon}_{GS,ES_{e,h}}}} f_{e,h}(\varepsilon) d\varepsilon. \quad (12)$$

In our model, the total carrier density per unit area (n, p_{unconf}) in the delocalized states (i.e., ES poorly confined in the dashes plus WL) has been calculated assuming a two dimensional density of states with an energy $\overline{\varepsilon_{2D_{e,h}}}$ and an equivalent effective mass $m_{2D_{e,h}}$, obtained by a proper fitting of the unconfined states energy band diagram (see Section III-A). The carrier density is then

$$n, p_{unconf} = \int_{\bar{\varepsilon}_{2D_{e,h}}}^{\infty} \frac{m_{2D_{e,h}}}{\pi\hbar^2} f_{e,h}(\varepsilon) d\varepsilon. \quad (13)$$

Finally, $n, p_{barrier}$ is the total number of carriers per unit area in the barrier of thickness $d_{barrier}$ and are calculated assuming
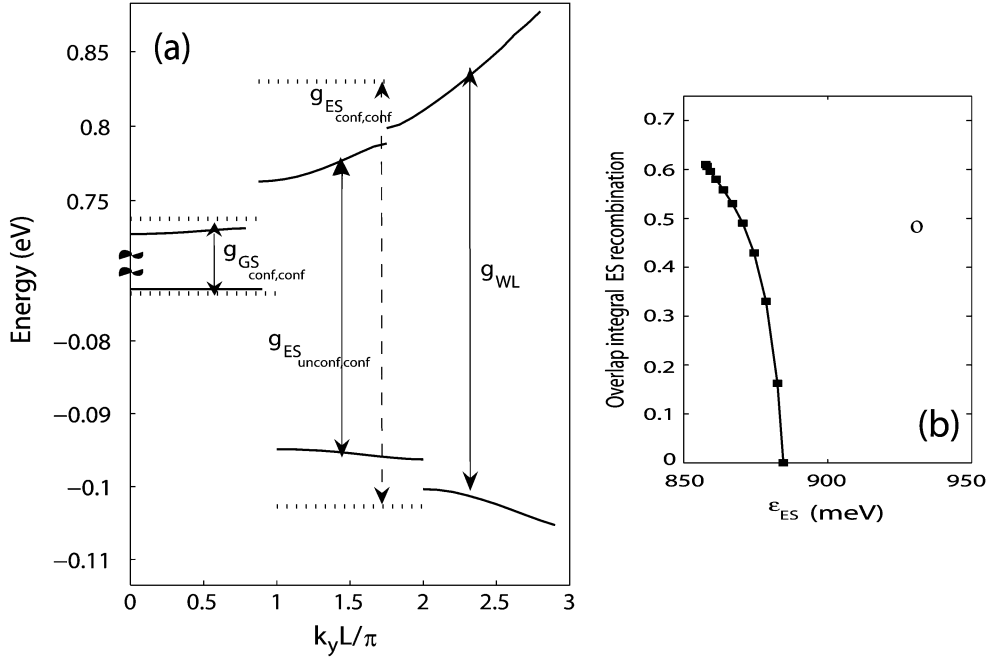
Fig. 4. (a) Recombination between CB and VB states with the corresponding contribution to the gain in the case of the single isolated dash model (dashed line) and the dash coupling with WL model (solid line). (b) Overlap integrals between the ES electron and hole envelope functions ($\psi_{e,h}(x,y)$) versus the ES recombination energy (ε_{ES}); empty circle: single isolated dash model; line with bold squares: dash coupling and WL model.

a three dimensional density of states (carrier unconfined in all directions)

$$n, p_{\text{barrier}} = d_{\text{barrier}} \frac{1}{2\pi^2} \left(\frac{2m_{e,h_{\text{barrier}}}}{\hbar^2} \right)^{3/2} \times \int_{\varepsilon_{c,v}}^{\infty} \sqrt{\varepsilon - \varepsilon_{c,v}} f_{e,h} d\varepsilon \quad (14)$$

with $m_{e,h_{\text{barrier}}}$ the carrier effective mass in the InAlGaAs barrier and $\varepsilon_{c,v}$ the barrier conduction and valence band edge.

III. NUMERICAL RESULTS

From the numerical solution of the Schrödinger equation (1), we can obtain the CB and VB energies versus the momentum k_y, the wavefunctions $\psi_{n,k_{y_{e,h}}}(x,y)$, the recombination energies between the CB and VB states and the overlap integrals between the corresponding wavefunctions. The post-processing of these data allows to calculate the gain spectra and the carrier distribution according to the model presented in Section II-C and Section II-D.

In this section, we analyze the optoelectronic properties of the InAs–InAlGaAs QDash material reported in many recently realizations [7]. We will compare the results obtained with the model based on the assumption of single isolated dashes with those calculated with the more realistic model that includes the presence of the WL and the effects of the dash coupling. This comparison will highlight the importance of considering the more realistic structure, in order to predict correctly the gain performance and in particular the optical gain bandwidth. The proposed approach will then be used to design a modified QDash structure that should allow to increase significantly the optical gain bandwidth respect to the structures realized up to now [7]. The dash geometry used in our simulations is in Fig. 1(c) and the other material parameters are listed in Table I.

A. Energy Diagram and Density of States

As an example we compare in Fig. 2 the CB and VB energy diagram of the structure shown in Fig. 1(c). In the case of the single isolated dash there are two states both in CB and VB whose energy is independent on the wavenumber k_y. These states are indeed completely confined in the dashes; the GS wavefunction has an even symmetry in both x and y direction, whereas the ES has an odd symmetry in y.

Including the WL and the dash coupling we get significant changes of the energy diagram in the CB respect to the VB, due to the lighter electron effective mass. The GS in both CB and VB is still well confined: its energy is indeed practically independent on k_y and the associated wavefunctions are well inside the dash. The same behavior occurs for the ES in VB. On the contrary, in CB, the ES energy is strongly dependent on k_y with the formation of a mini-band ($\varepsilon_{ES,e}(k_y)$). The associated wavefuction shows that electrons are now poorly confined in the dashes and almost spread all over the WL. We also observe that the presence of the WL has negligible effect on the GS energy, but it significantly reduces the ES energy in both CB and VB.

The higher energy mini-bands shown in dashed line in CB and VB corresponds to the WL states, whose wavefunction are uniformly distributed in the WL. Even for these states the mini-band nature still persists, due to the periodic perturbation introduced by the dashes.

From the dispersion curves (energy versus k_y) of the unconfined states (ES and WL in CB, WL state in VB) shown in Fig. 2, we can extract the equivalent parameters ($m_{2D_{e,h}}$ and $\varepsilon_{2D_{e,h}}$) to be inserted in (13). We see that the unconfined states exist for energies higher than $\overline{\varepsilon_{2D_e}} = 312.5$ meV in CB and $\overline{\varepsilon_{2D_h}} = 100.3$ meV in VB. We show in Fig. 2(a) and (b) that a parabolic function (thin solid line) can fit quite well the band curvature of the unconfined states. From the curvature of the
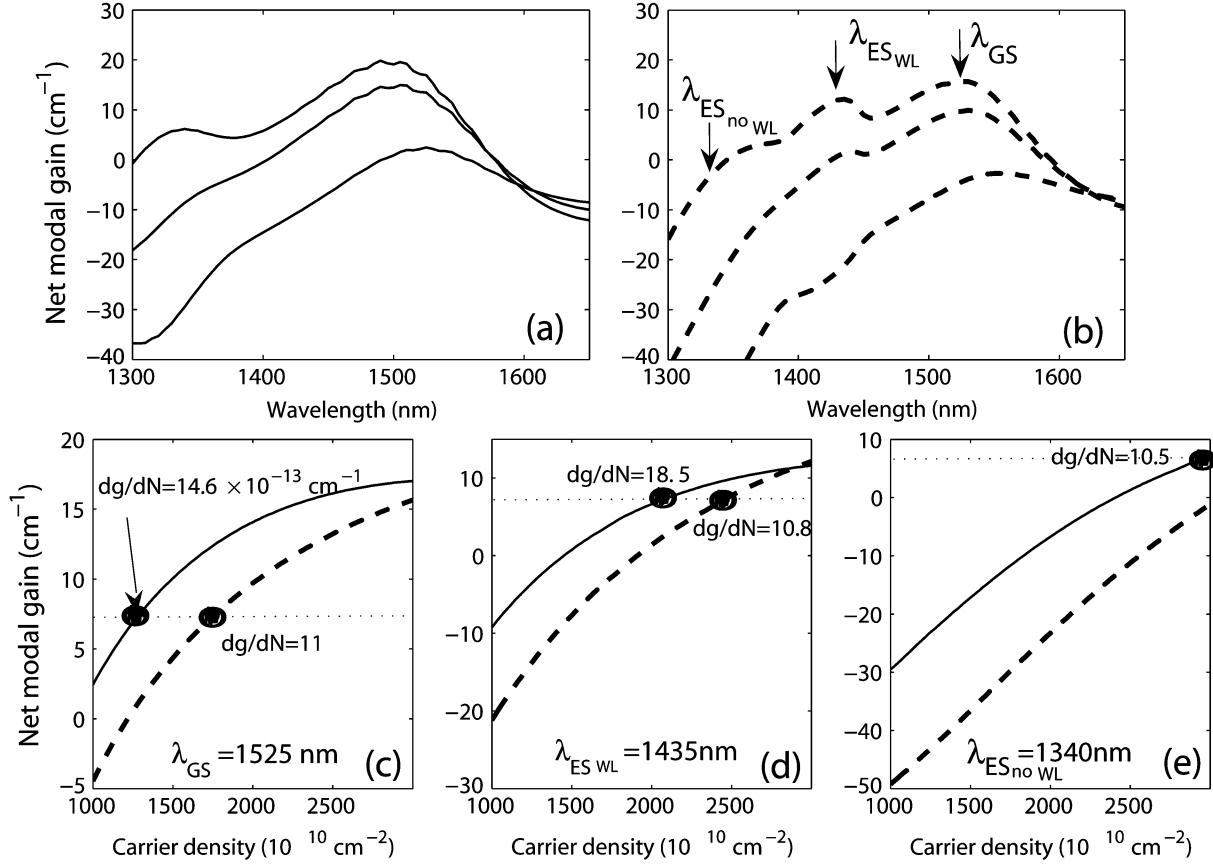
Fig. 5. (a) Net modal gain spectra calculated for the single isolated dash case (continuous line) and (b) including the WL and dash coupling (dashed line) at the same injected carrier densities of 1000, 2000, and $3000 \cdot 10^{10}$ cm^{-2}. (c)–(e) Net modal gain versus carrier density at the three wavelengths indicated by the arrows in (b). The dots in (c)–(e) corresponds to the threshold condition with $g_{th} = 7$ cm^{-1}; for each threshold point we also report the corresponding differential gain dg/dN.

parabola we obtain the equivalent effective mass for the 2-D states: $m_{2D_e} = 0.052 m_0$ and $m_{2D_h} = 0.38 m_0$ (with m_0 the free electron mass). Approximating the unconfined state dispersion relation with a continuous parabola, we neglect the presence of the energy-gap among the mini-bands. Such approximation is however correct when, as in this case, this energy gap is much narrower than the mini-band width.

The formation of mini-bands caused by the WL have immediate impacts on the density of available states for the injected carriers in CB and VB. In Fig. 3 we show the density of states (DOS) in CB and VB calculated numerically from the energy diagrams in Fig. 2. In the case of the single isolated dash model [Fig. 3(a) and (b)], both GS and ES DOS in CB and VB have the $1/\sqrt{\varepsilon}$ shape, typical of the quantum wire material.

Including the WL and the dash coupling, the ES energy in CB spreads over a wide range, getting practically continuous to the WL band [see Fig. 2(a)]. As a consequence the sum of the ES DOS with the WL DOS gives approximately a step-like function (Fig. 3(c)), typical of a 2-D material. On the contrary in VB the DOS of the ES state maintains the $1/\sqrt{\varepsilon}$ shape even in presence of the WL [Fig. 3(d)]. In this case, the additional step-like DOS is only due to the WL states.

B. Gain Performance

From the numerical results obtained in the previous section we could evaluate the gain performance according to the model presented in Section II-C. The energy band diagram in Fig. 4(a) shows the various contribution to the gain as indicated in (2); we see that in the case with WL and dash coupling, the ES contribution is due to recombination between mini-band states in CB and confined states in VB. Since the contribution to the gain spectrum is also proportional to the overlap integral between the electron and hole envelope functions $(\psi_{e,h}(x,y))$, we plot in Fig. 4(b) the overlap integral for the ES recombination calculated with the two models. As shown in Fig. 4(b), the WL and the dash coupling causes the ES overlap integral to be dependent on the ES recombination energy and smaller than in the single isolated dash case. For the GS contribution, we have seen only slight differences between the two models with values of overlap integral of about 0.7. We, therefore, expect that the more realistic model including the WL will give smaller gain at the ES recombination energies with significant impact on the maximum gain, on the differential gain and on the gain bandwidth.

The corresponding net modal gain spectra are shown in Fig. 5(a) and (b). In order to compare the gain performance obtained using the two models, we calculated the net modal gain versus the total injected carrier density at three wavelengths: $\lambda_{GS} = 1525$ nm [Fig. 5(c)], $\lambda_{ES_{WL}} = 1435$ nm [Fig. 5(d)], and $\lambda_{ES_{noWL}} = 1340$ nm [Fig. 5(e)]. The selected wavelengths correspond, respectively to the peak gain of the GS and ES emission with WL (λ_{GS} and $\lambda_{ES_{WL}}$) and to the peak of the ES emission in the single isolated dash ($\lambda_{ES_{no\ WL}}$).
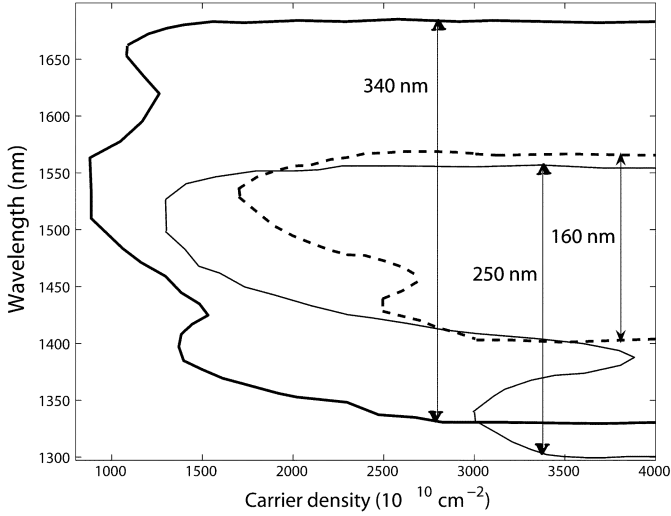
Fig. 6. Optical gain bandwidth calculated for $g_{th} = 7$ cm^{-1} and using the single isolated dash model (solid line) and the dash coupling with WL model (dashed line). The thick solid line is the bandwidth of the QDash structure designed in Section III-C for very broad optical bandwidth. At a fixed carrier injection, the bandwidth ($g_{net} \geq g_{th}$) is the wavelength range limited by the each curve.

Fig. 5(c)–(e) shows that the single isolated dash model always overestimates the gain and the differential gain. For example, fixing a threshold gain value of $g_{th} = 7$ cm^{-1}, the differential gain at threshold in Fig. 5(c)–(e) is always smaller in presence of the WL and dash coupling.

In order to understand if the quantum mechanical coupling or the presence of the WL are equally important in determining the gain spectra, we have also calculated the material gain increasing the separation between dashes and, therefore, decreasing the coupling effects. The results obtained have shown that the gain spectrum due to GS emission [gain around the peak λ_{GS} in Fig. 5(b)] is practically independent on the strength of the quantum mechanical coupling and it is exclusively dependent on the presence of the WL. On the contrary the gain due to the ES contribution [gain around the peak $\lambda_{ES_{WL}}$ in Fig. 5(b)] is strongly affected by the coupling effects; in particular as the coupling strength reduces the peak moves toward longer wavelength, its width narrows and its maximum decreases. From this analysis we, therefore, conclude that the coupling effect has at least to be included in the calculation of gain at high carrier injections, when also the ES starts being populated.

Finally, we quantitatively compare the gain performance in terms of available optical gain bandwidth. We define the gain bandwidth at a fixed carrier injection as the wavelength range where the net modal gain exceeds the threshold value g_{th}. In Fig. 6, we report the gain bandwidth versus carrier injection calculated with in the two cases previously considered. In the case of the single isolated dash the maximum gain bandwidth is rather wide (about 250 nm), thanks to the well wavelength separated contribution of GS and ES recombination. Including the WL and the dash coupling the maximum optical bandwidth reduces to about 160 nm because the ES contribution is not enough separated from the GS emission and also the values of the ES gain are smaller. This last result is in good agreement with the gain bandwidth measured in the QDash material realized up to now (NetTest) and clearly shows that the presence of
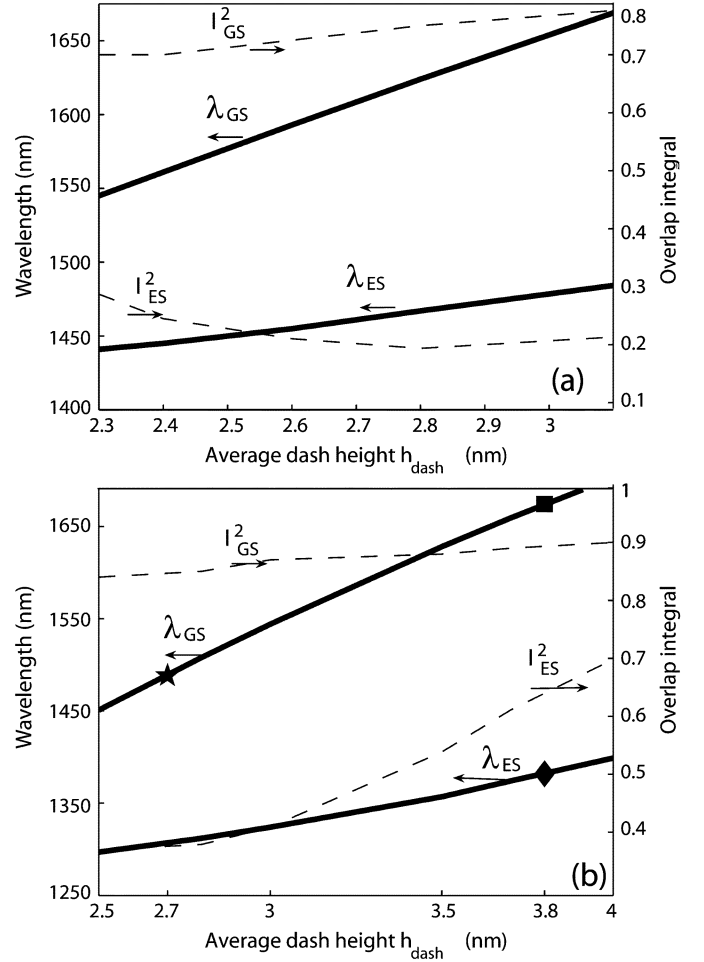

Fig. 7. Emission wavelength from the GS (λ_{GS}) and ES (λ_{ES}) and corresponding overlap integrals (I^2_{GS} and I^2_{ES}) versus the dash average height calculated with the model including WL and dash coupling for a QDash structure with (a) In$_{0.528}$Al$_{0.238}$Ga$_{0.234}$As and (b) In$_{0.522}$Al$_{0.4}$Ga$_{0.078}$As barrier. The symbols evidence the emission wavelength of from the two QDash layers chosen for the wide bandwidth design.

the WL and the high dash density are the major limitations to a very broad-band optical gain.

C. Design Proposal for Extended Gain Bandwidth

From the results shown in Fig. 6, it is clear that the QDash material could be used for wide optical gain spectra, provided that the influence of the WL and the dash coupling is reduced. Since the WL can not be eliminated by the technological process and the high dash density is necessary to reach enough modal gain, we have used our numerical model to investigate new QDash structures that allow to achieve a broader emission even in presence of the WL and the high dash concentration. The target is covering the whole wavelength range 1360–1675 nm from the E-band to the U-band of the optical communication systems.

A first solution could be an increase of the width of inhomogeneous broadening spectrum by growing QDash layers of different average height, such that each layer covers a different portion of the wavelength range [26]. In Fig. 7(a), we report the results for the GS (λ_{GS}) and the ES (λ_{ES}) emission wavelength calculated for various dash height considering in the simulation the WL and the dash coupling. The figure shows that the GS
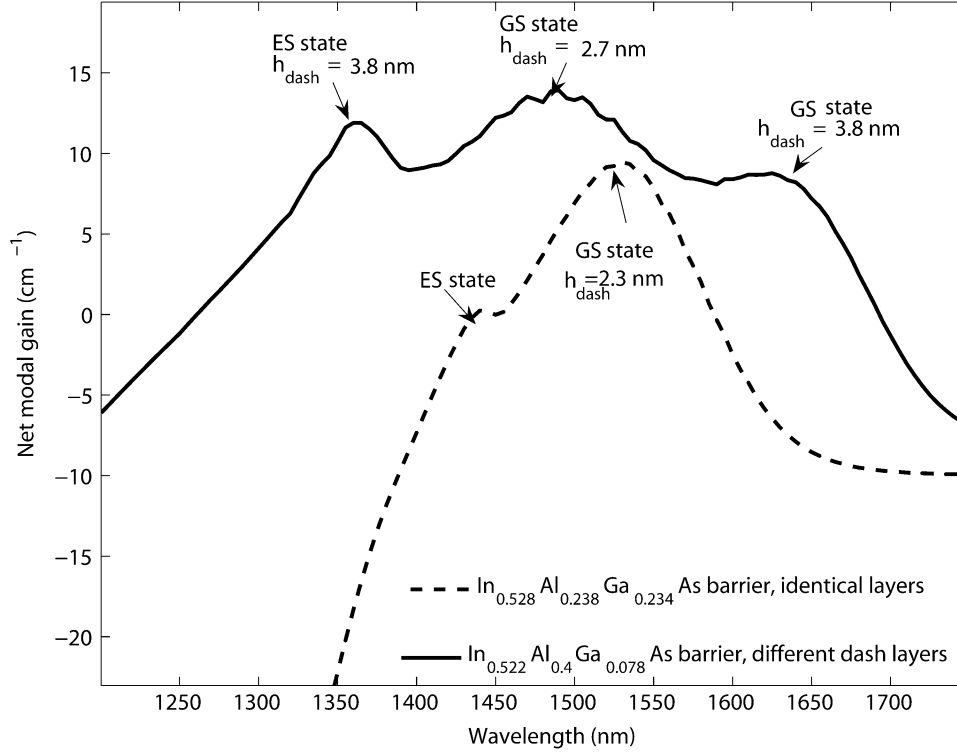
Fig. 8.   Comparison between the calculated gain spectra of the structure with $In_{0.528}Al_{0.238}Ga_{0.234}As$ barrier and four identical dash layers ($h_{\mathrm{dash}} = 2.3$ nm) [2] and the structure with $In_{0.522}Al_{0.4}Ga_{0.078}As$ barrier and four layers identical two by two ($h_{\mathrm{dash}} = 2.7$ nm and $h_{\mathrm{dash}} = 3.8$ nm). In the figure, the contribution to the gain from the various GS and ES transitions and from the various layers are shown.

emission from the different layers could cover the long wavelength range 1550–1650 nm, thanks to the significant shift of λ_{GS}, but the ES emission wavelength only varies from 1440 to 1460 nm. In any case, it is not possible covering the short wavelength range 1300–1440 nm because we can not reduce further the dash height. From the values of the overlap integral reported in Fig. 7(a) we also see that the ES emission, essential to cover the short wavelength range, is still quite inefficient for any dash height used. This design also requires a precise control of the average dash height in a narrow range (2.3–3 nm) and this may be quite difficult using a self-assembled growth process.

The solution we found to overcome these problems consists in increasing the aluminum concentration of the InAlGaAs barrier, in order to increase the energy depth of the barrier. In Fig. 7(b), we report λ_{GS} and λ_{ES} versus the dash height for a structure with an $In_{0.522}Al_{0.4}Ga_{0.078}As$ barrier. In this case, λ_{GS} shifts from 1450 to 1650 nm and λ_{ES} shifts from 1270 to 1370 nm, (covering all the short wavelength region) with a variation of h_{dash} between 2.5 and 4 nm. Furthermore, using a deeper barrier and thicker dashes, the ES emission is more efficient than in the previous case, as demonstrated by the corresponding overlap integrals reported in Fig. 7(b).

Based on these considerations and the results in Fig. 7(b), we have designed a new QDash structure with $In_{0.522}Al_{0.4}Ga_{0.078}As$ barrier and four dash layers equal two by two. We have chosen two layers with average dash height $h_{\mathrm{dash}} = 2.7nm$, because the corresponding GS emission [star symbol in Fig. 7(b)] falls in the central part of the target wavelength, and two layers with $h_{\mathrm{dash}} = 3.8$ nm having the GS and ES emission, respectively in the longer and shorter

wavelength side of the spectrum [square and diamond symbol in Fig. 7(b)].

We report in Fig. 8, the net modal gain spectrum calculated for a total injected carrier density of $2 \cdot 10^{13}$ cm^{-2}; the comparison with the spectrum of the structure analyzed in Section III-B clearly shows a significant improvement of the optical gain bandwidth. We also observe that even if the inhomogeneous gain broadening is increased using dash layers of different thickness, the maximum gain is not reduced because the deeper energy barrier allows a more efficient capture of the carriers in the dashes instead in the WL or barrier state. This also reflects on the resulting gain bandwidth shown in Fig. 6 in thick solid line: the bandwidth fully covers the target range 1360–1675 nm and it is very wide even at lower carrier injection respect to the case with barrier having 0.24 aluminum composition as in the realized structures [2].

IV. CONCLUSION

We have presented a numerical model for the self-consistent calculation of the gain characteristics of a QDash active material including the presence of the WL and the quantum mechanical coupling among adjacent dashes. The numerical tool was used to compare the energy band diagrams, the density of states and the gain spectra calculated with this more realistic model with those obtained assuming only single isolated dashes without WL. This comparison has shown that the presence of the WL causes a reduction of the gain performance and in particular of the differential gain and the available optical gain bandwidth. From this analysis we found that an improved QDash material can be obtained increasing the aluminum concentration of

the InAlGaAs barrier and growing dash layers of different dash thickness.

REFERENCES

[1] M. Grundmann, *Nano-Optoelectronics*. Berlin, Germany: Springer-Verlag, 2002.

[2] R. Schwertberger, D. Gold, J. Reithmaier, and A. Forchel, "Long-wavelength InP-based quantum dash lasers," *IEEE Photon. Technol. Lett.*, vol. 14, no. 6, pp. 735–737, Jun. 2002.

[3] P. Bharracharya, *J. Phys. D, Special Issue on Self-Organized Quantum Dots*, vol. 38, no. 13, Jul. 2005.

[4] L. H. Li, M. Rossetti, A. Fiore, L. Occhi, and C. Velez, "Wide emission spectrum from superluminescent diodes with chirped quantum dot multilayers," *IEEE Electron. Lett.*, vol. 41, no. 1, pp. 540–542, Jan. 2005.

[5] H. Li, G. Liu, P. Varangis, T. Newell, A. Stintz, B. Fuchs, K. Malloy, and L. Lester, "150-nm tuning range in a grating-coupled external cavity quantum-dot laser," *IEEE Photon. Technol. Lett.*, vol. 12, no. 7, pp. 759–761, Jul. 2000.

[6] T. Akiyama, M. Ekawa, M. Sugawara, K. Kawaguchi, H. Sudo, A. Kuramata, H. Ebe, and Y. Y. Arakawa, "An ultrawide-band semiconductor optical amplifier aaving an extremely high penalty-free output power of 23 dbm achieved with quantum dots," *IEEE Photon. Technol. Lett.*, vol. 17, no. 8, pp. 1614–1616, Aug. 2005.

[7] J. P. Reithmaier, A. Somers, S. Deubert, R. Schwertberger, W. Kaiser, A. Forchel, M. Calligaro, P. Resneau, O. Parillaud, S. Bansropun, M. Krakowski, R. Alizon, D. Hadass, A. Bilenca, H. Dery, V. Mikhelashvili, G. Eisenstein, M. Gioannini, I. Montrosset, T. W. Berg, M. van der Poel, J. Mørk, and B. Tromborg, "Inp based lasers and optical amplifiers with wire-/dot-like active regions," *J. Phys. D*, vol. 38, no. 13, pp. 2088–2102, Jul. 2005.

[8] B. Stintz, P. Varangis, K. Malloy, L. Lester, T. Newell, and H. Li, "Quantum Dash Devices," U.S. Patent 6 600 169, Jul. 29, 2003.

[9] P. V. an H. Li, G. L. T. Newell, A. Stintz, B. Fuchs, K. Malloy, and L. Lester, "Low-threshold quantum dot lasers with 201 nm tuning range," *IEEE Electron. Lett.*, vol. 36, no. 18, pp. 1544–1545, Aug. 2000.

[10] O. Kwon, K. Kim, E. Sim, J. Kim, H. Kim, and K. Oh, "Asymmetric multiple-quantum-well laser diodes with wide and flat gain," *Opt. s Lett.*, vol. 28, no. 22, pp. 2189–2191, Nov. 2003.

[11] H. Johnson, V. Nguyen, and A. Bower, "Simulated self-assembly and optoelectronic properties of inas/gaas quantum dot array," *J. Appl. Phys.*, vol. 92, no. 8, pp. 4653–4663, Oct. 2002.

[12] D. R. Matthews, H. Summers, P. Smowton, and M. Hopkinson, "Experimental investigation of the effect of the wetting-layer states on gain-current characteritic of quantum-dot lasers," *Appl. Phys. Lett.*, vol. 81, no. 26, pp. 4904–4906, Dec. 2002.

[13] H. Dery and G. Eisenstein, "The impact of energy band diagram and inhomogeneous broadening on the optical differential gain in nanostructure lasers," *IEEE J. Quantum Electron.*, vol. 41, no. 1, pp. 26–35, Jan. 2005.

[14] R. Melkin and M. Willatzen, "Band structure of conical quantum dots with wetting layer," *Nanotechnology*, vol. 15, no. 1, pp. 1–8, Jan. 2004.

[15] L. Asryan and S. Luryi, "Effect of internal optical loss on threshold characteristics of semiconductor lasers with a quantum-confined active region," *IEEE J. Quantum Electron.*, vol. 40, no. 7, pp. 833–843, Jul. 2004.

[16] M. Gioannini, "Numerical modeling of the emission characteristics of semiconductor quantum dash materials for lasers and optical amplifiers," *IEEE J. Quantum Electron.*, vol. 40, no. 4, pp. 364–373, Apr. 2004.

[17] D. Bimberg, M. Grundman, and N. Ledenstov, *Quantum Dot Heterostructures*. Chichester, U.K.: Wiley, 1999.

[18] next$\mathbf{nano}^3$ Device Simulation Package (2002). [Online]. Available: http://www.wsi.tum.de/nextnano3/

[19] H. Dery, E. Benisty, A. Epstein, V. Mikhelashvili, G. Eisenstein, R. Schwertberger, D. Gold, J. Reithmaier, and A. Forchel, "On the nature of quantum dash structure," *J. Appl. Phys.*, vol. 95, no. 11, pp. 6103–6111, Jun. 2004.

[20] D. Deppe, D. Huffaker, S. Csutak, Z. Zou, G. Park, and O. Shchekin, "Spontaneous emission and threshold characteristics of 1.3-μm InGaAs-GaAs quantum dot GaAs-based laser," *IEEE J. Quantum Electron.*, vol. 35, no. 8, pp. 1238–1246, Aug. 1999.

[21] P. Blood, "On the dimensionality of optical absorption, gain and recombination in quantum-confined structures," *IEEE J. Quantum Electron.*, vol. 36, no. 3, pp. 354–362, Mar. 2000.

[22] J. Piprek, *Semiconductor Optoelectronic Devices*. San Diego, CA: Academic, 1996.

[23] P. Zory, *Quantum Well Lasers*. San Diego, CA: Academic, 1993.

[24] M. Sugawara, *Self-Assembled InGaAs–GaAs Quatum Dots*. San Diego, CA: Academic, 1999.

[25] D. G. Deppe, H. Huang, and O. Shchekin, "Modulation characteristics of quantum-dot lasers: The influence of p-type doping and the electronic density of states on obtaining high speed," *IEEE J. Quantum Electron.*, vol. 38, no. 12, pp. 1587–1593, Dec. 2002.

[26] A. Sommers, C. Weichelr, R. Schwertberger, J. Reithmaier, and A. Forchel, "Tailored inp-based quantum dash structures for ultra-wide gain bandwidth applications," in *Proc. 16th Conf. Indium Phosphide and Related Materials*, Kagoshima, Japan, 2004, Paper TuA3.

Mariangela Gioannini was born in Cuorgnè, Italy, in 1973. She received the M.S. degree in electronic engineering and the Ph.D. degree in electronic and communication engineering from Politecnico di Torino, Torino, Italy in 1998 and 2002, respectively.

Since 2002, she has been with the Dipartimento di Elettronica of Politecnico di Torino, first with a postdoctoral position and then as permanent Researcher since January 2005. She was a Visiting Researcher at the Univesity of Bristol, Bristol, U.K. in 2001 and at the Fraunhofer Institut für Nachrichtentechnik, Heinrich-Hertz-Institut, Berlin, Germany, in 2001 and 2002. Her research interests involve modeling and characterization of semiconductor lasers and optical amplifiers. Since 2002, her main research activity has been focused on modeling of quantum-dot and quantum-dash materials, lasers, and optical amplifiers.